Methionine – Supplementary Material

I: Evaluation of $^{3}J_{CSCC}$ using alternate theoretical models.

Figure S1:

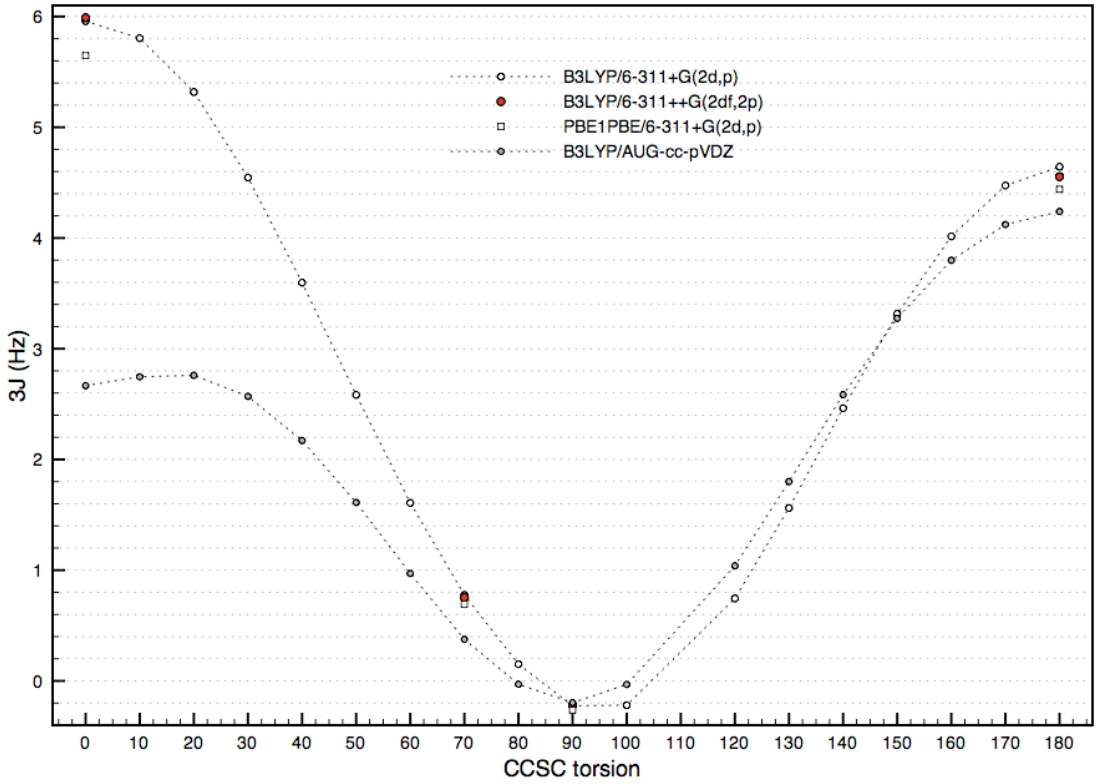

The figure shown above compares calculated $^{3}J_{CSCC}$ values determined for the model compound ethyl methyl sulfide (EMS). The calculations cover the full torsional range for the B3LYP/6-311+G(2d,p) and B3LYP/AUG-cc-pVDZ levels of theory, and include a few additional values calculated using two other models: B3LYP/6-311++G(2df,2p) and PBE1PBE/6-311+G(2d,p). As is apparent from the figure, three of the basis sets yielded similar results, while the results obtained using B3LYP/AUG-cc-pVDZ differ significantly. The latter calculations also do not give a good fit to a Karplus relation, requiring an additional introduction of a sin(θ) term in order to fit the decreasing values predicted near θ = 0. However, nearly all of the significant discrepancies are for very small angles, which are largely excluded from most experimental data since such values are energetically unfavorable. Overall, the results for all four models are in good agreement for the energetically favored conformational space. As noted in the text, the calculations using B3LYP/6-311+G(2d,p) were consistently found to provide the best fit for the available model compounds.

II: Calculated $^3J_{CSCH}$ coupling constants at the B3LYP/6-311+G(2d,p) level of theory as as a function of the absolute value of the subtended dihedral angle.

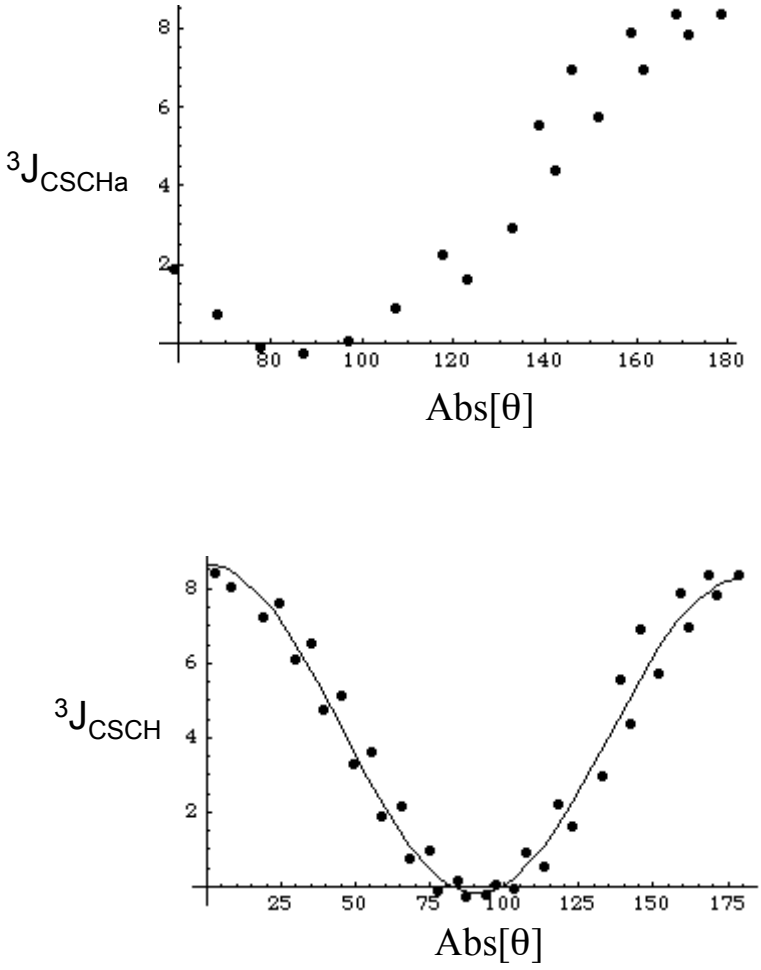

Figure S2. The figures above illustrate that the $^3J_{CSCH}$ is not an even function of θ, i.e., $^3J_{CSCH}(\theta) \neq {}^3J_{CSCH}(-\theta)$. This is particularly apparent when only one of the protons is considered, as in the top figure. This behavior requires a modification of the Karplus relations such as that described in the text.

III: Comparison with Tvaroska Data and Tafazzoli calculations

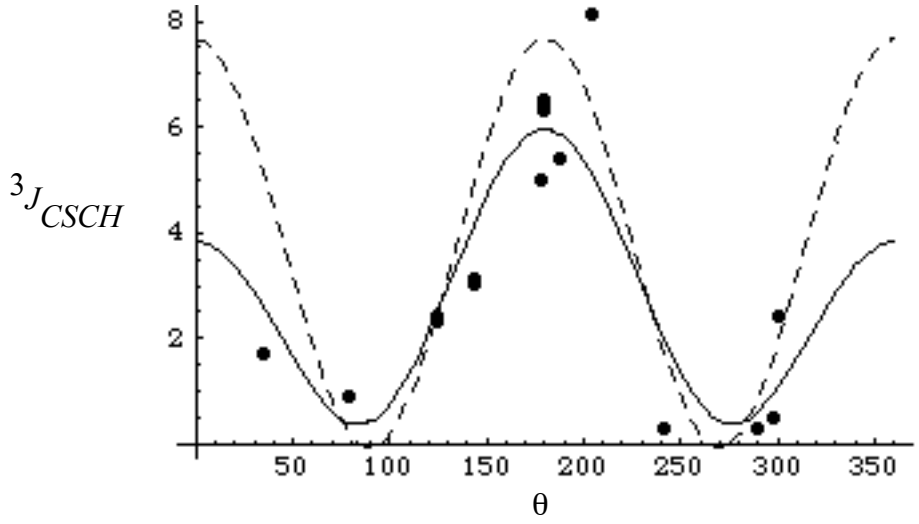

Figure S3. The plot shown above summarizes the data in Table 1 of Tvaroska et al. (Carbohydrate Res. 229, 225-231; 1992) (filled circles), the dihedral angle dependence which they obtained based on this data (solid line and Eq. 8 in the accompanying manuscript), and the curve obtained here for the Karplus relation describing the average shift of the two protons (dashed line and Eq. 7 in the accompanying manuscript):

$$^3J_{CSCH}(Tvaroska) = 0.45 - 1.06 + 0.216Cos\theta + 4.44Cos^2\theta \qquad [S1]$$

and

$$^3J_{CSCH}(mean) = -0.05 + 7.7Cos^2\theta \qquad [S2]$$

We also note here the calculated values for the coupling constants in Table 4 of the study by Tafazzoli and Ghiasi (Carbohydrate Res. 342, 2086-2096; 2007) are inconsistent with the plots shown in Figure 8 of that reference, and our fit of the calculated coupling constant results in Table 4 resulted in dramatically different Karplus relations for $^3J_{CSCH}$, $^3J_{COCH}$, and $^3J_{CCCH}$ than are presented in that reference.

IV: Isotropic and anisotropic shielding parameters for the S-CH_3 carbon of EMS were calculated at the B3LYP/6-311+G(2d,p) (left two columns) and B3LYP/6-311++G(2df,2p) (right two columns) levels of theory. The calculated isotropic shielding using the two approaches is nearly identical:

Torsion θ	B3LYP/6-311+G(2d,p)		B3LYP/6-311++G(2df,2p)	
	Isotropic	Anisotropy	Isotropic	Anisotropy
0	167.3347	23.7538	167.2768	22.9909
10	167.1926	23.6338	167.1644	22.8712
20	166.9307	23.4888	166.9375	22.7628
30	166.6592	23.6912	166.6861	23.0279
40	166.3020	24.8190	166.3373	24.2040
50	165.6761	27.1431	165.7022	26.5587
60	164.7811	30.3064	164.8023	29.6814
70	163.6403	33.1281	163.6633	32.4774
80	162.3215	34.7888	162.3361	34.1351
90	160.9211	35.7356	160.9372	35.0969
100	159.9692	36.1847	159.9824	35.5595
110	159.2968	36.4819	159.3182	35.8987
120	159.0658	36.4987	159.0673	36.0196
130	159.0168	36.4093	158.9957	35.9513
140	159.1604	36.2077	159.1131	35.7384
150	159.4330	35.9825	159.3881	35.4701
160	159.7916	35.8221	159.7622	35.2652
170	160.1356	35.7185	160.1264	35.1070
180	160.2685	35.6998	160.2704	35.0696

V. Conformation of Free Methionine

We sought to further evaluate the conformation of free methionine using both the $^3J_{C_\beta C_\varepsilon}$ and $^3J_{C_\varepsilon H_\gamma}$ coupling constants, measured as 1.55 Hz and 4.4 Hz, respectively. Although due to the chiral center at Cα, the probabilities and energy minima of the two gauche conformations, defined below, are not identical, the Ha and Hb resonances were not individually assigned, and the data were fit by assuming conformations 1 and 3, defined in the diagram below, are symmetric and equally populated.

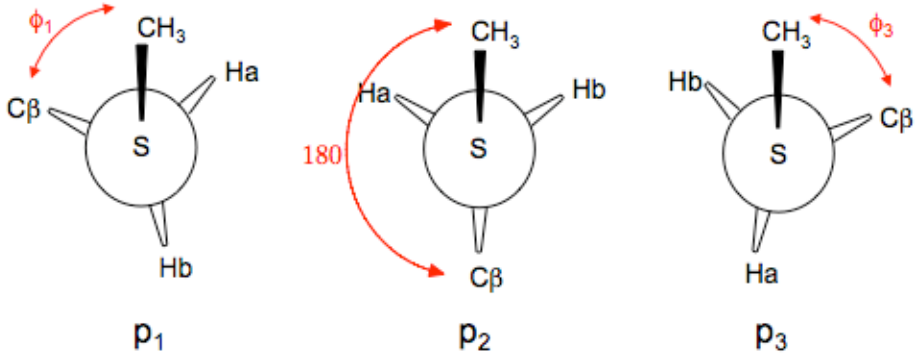

The three experimental parameters: $^3J_{CSCC}{}^{exp}$, $^3J_{CSCHa}{}^{exp}$, and $^3J_{CSCHb}{}^{exp}$, plus a normalization condition are insufficient for determining the five parameters: p_1, p_2, p_3, ϕ1 and ϕ3. However, based on the assumption of symmetry discussed above, we have used the approximations: $\phi_3 = -\phi_1$, and $p_1 = p_3 = \frac{1}{2}(1-p_2)$, leaving only two parameters, ϕ_1 and p_2 to be determined using the equations below:

$$
\begin{aligned}
{}^3J_{CSCC}{}^{exp} &= p_1{}^3J_{CC}(\phi_1) + p_2{}^3J_{CC}(180) + p_3{}^3J_{CC}(\phi_3) \\
{}^3J_{CHa}{}^{exp} &= p_1{}^3J_{CSCHa}(\phi_1 + 120) + p_2{}^3J_{CSCHa}(-60) + p_3{}^3J_{CSCHa}(\phi_3 + 120) \qquad \text{[S3]} \\
{}^3J_{CHb}{}^{exp} &= p_1{}^3J_{CSCHb}(\phi_1 - 120) + p_2{}^3J_{CSCHb}(60) + p_3{}^3J_{CSCHb}(\phi_3 - 120)
\end{aligned}
$$

In the above expressions, the selection of the correct equation for $^3J_{CSCHa}$ and $^3J_{CSCHb}$ is based on the calculation requiring that $^3J_{CSCHa}(-60°) < {}^3J_{CSCHa}(+60°)$ and conversely, $^3J_{CSCHb}(-60°) > {}^3J_{CSCHb}(+60°)$. Following this procedure, the second and third equations given above become identical. Setting $^3J_{CSCC} = 1.55$ Hz and $^3J_{CSCHa} = {}^3J_{CSCHb} = 4.4$ Hz, the above equations define curves that depend on the parameters p_2 and ϕ3. The intersection of these curves defines the parameter values that satisfy both of the coupling constant constraints. A plot of the two curves is shown below in panel a of Figure S4. From this figure, it is apparent that the two curves for $^3J_{CSCHa/b}$ and $^3J_{CSCC}$ do not intersect until $\phi \sim 100°$, at which the three fractional populations approach a limiting value of $p_1 = p_2 = p_3 = 1/3$. This solution is in poor agreement with the energy minimum predicted for the model EMS compound which, as discussed in the text, predicts a ϕ_g minimum near 67°, and a fractional trans probability of ~ 0.2. A somewhat improved result was obtained by using Equation 6 for the average coupling constant with Ha and Hb, rather

than the two separate expressions for $^3J_{CSCHa}$ and $^3J_{CSCHb}$. In this case, the curves intersect at $\phi \sim 80°$, with p_2 still = ~ 1/3 (panel b of Figure S4, below).

One basis for this discrepancy is probably the broad minima around the stable, staggered conformations, so that the nominally *gauche* and *trans* rotamers represent thermal averaging covering ±15 to 25°. Improved agreement with theory could be obtained by introducing additional offset angles so that, e.g., the trans conformation corresponds to 160° rather than to 180°. In addition, the results were found to be extremely sensitive to the coupling constant values. Much closer agreement with the theoretical results for EMS were obtained using Eq. 5 and increasing the $^3J_{CSCH}^{exp}$ value by 7 %, or by using Eq. 6 and increasing the $^3J_{CSCH}^{exp}$ value by 3 %. This approach yielded ϕg values near 70° and p_2 values of 0.22 and 0.21, respectively. The two results are shown in panels c and d in figure S4 below:

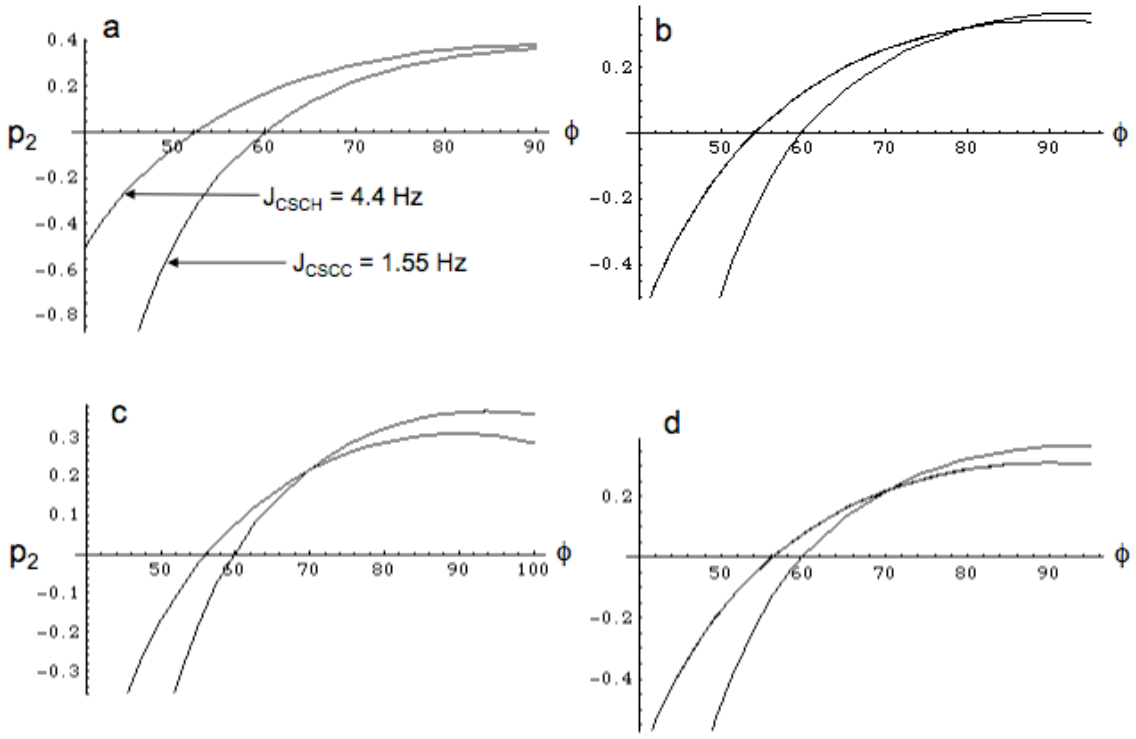

Figure S4. Analysis of methionine coupling data. The two curves correspond to the equations given above for $^3J_{CSCC}$ and $^3J_{CSCHa} = {}^3J_{CSCHb}$ considered as a function of the fractional trans concentration p_2 and the gauche angle ϕ. a) Data fit using equations 3 and 5 from the text. b) analogous calculations using equations 3 and 6; c) fits obtained using equations 3 and 5, and increasing the experimental $^3J_{CSCH}$ value by 7 %; d) fit obtained using equations 3 and 6, and increasing the experimental $^3J_{CSCH}$ value by 3 %.

VI: Methionine χi values during an Amber simulation of the calmodulin-*M13* complex.

The calculations below correspond to the three χi values for each calmodulin methionine residue in the Amber simulations of the calmodulin-*M13* complex. The calculations began with structure 2BBM, and the data shown correspond to a 16 ns simulation period beginning 14 ns after the simulations were initiated. A few of the periods during which methionine residues adopted an mmp conformation are indicated with red rectangles. The χ3 values observed during these periods are atypically large, ~ 100°.

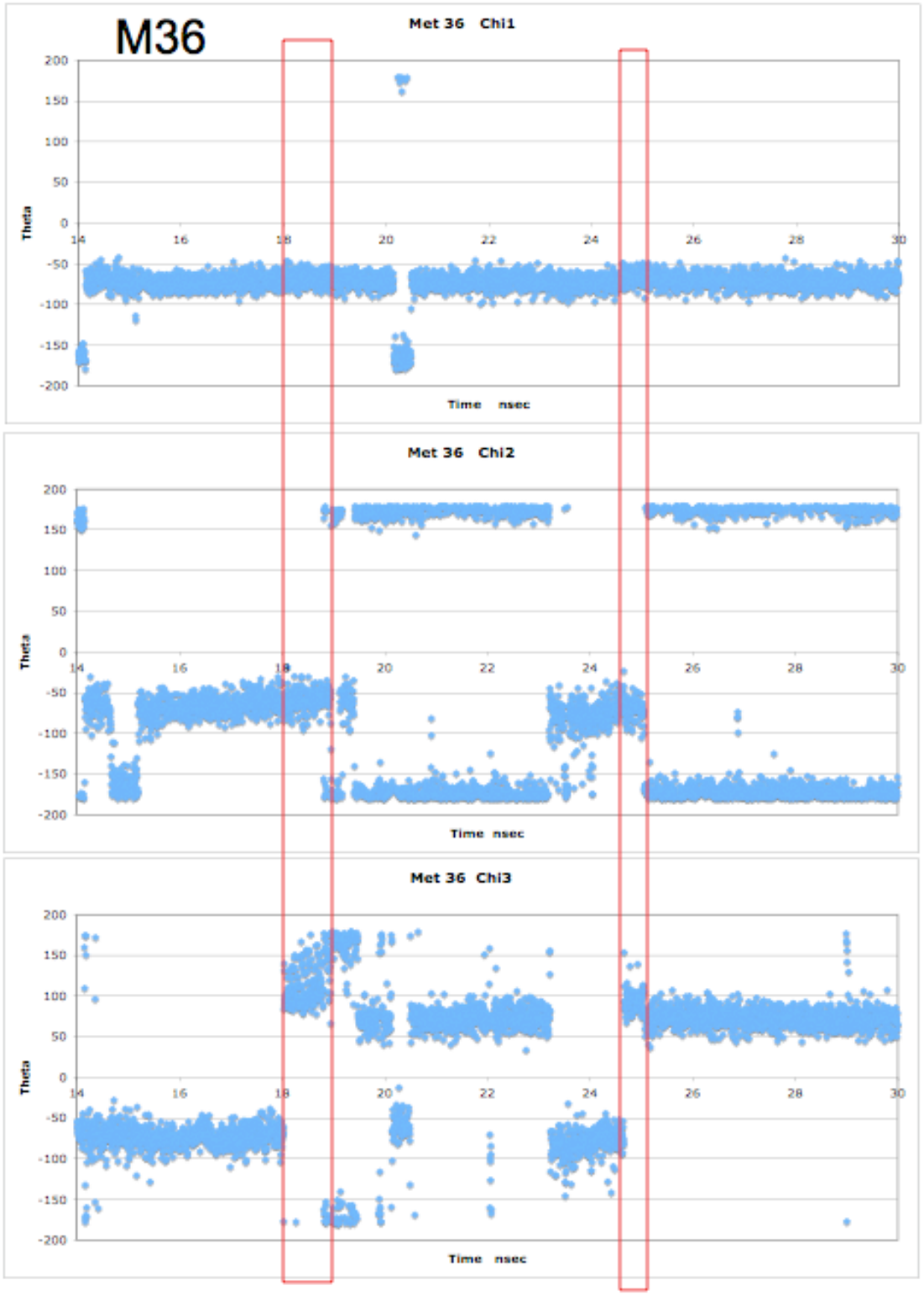
M36
Met 36 Chi1
Theta
Time nsec
Met 36 Chi2
Theta
Time nsec
Met 36 Chi3
Theta
Time nsec

M51

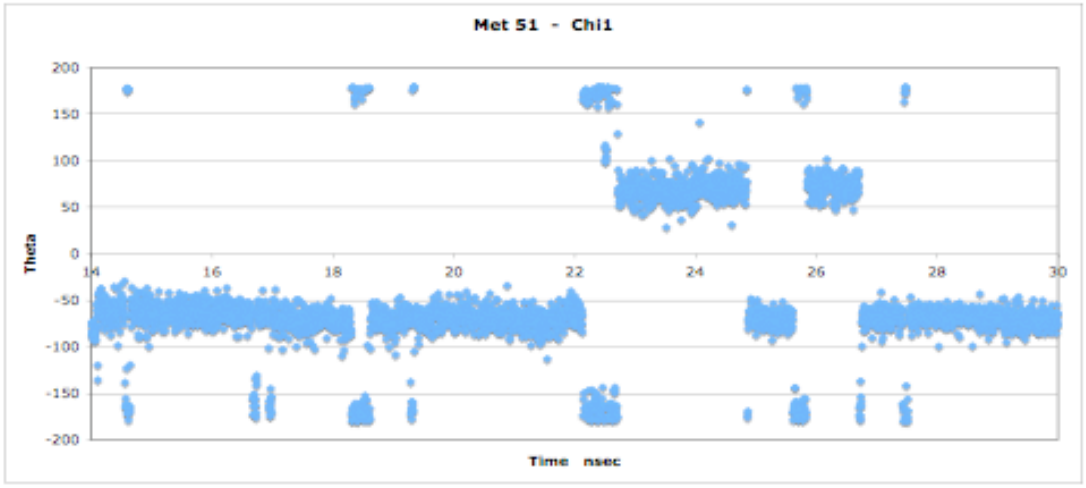
Met 51 - Chi1
Theta
Time nsec

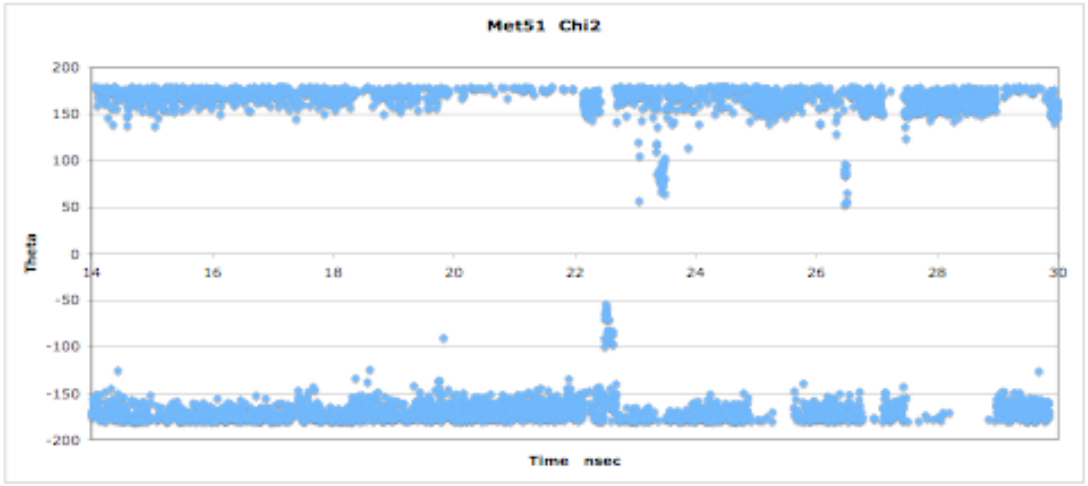
Met51 Chi2
Theta
Time nsec

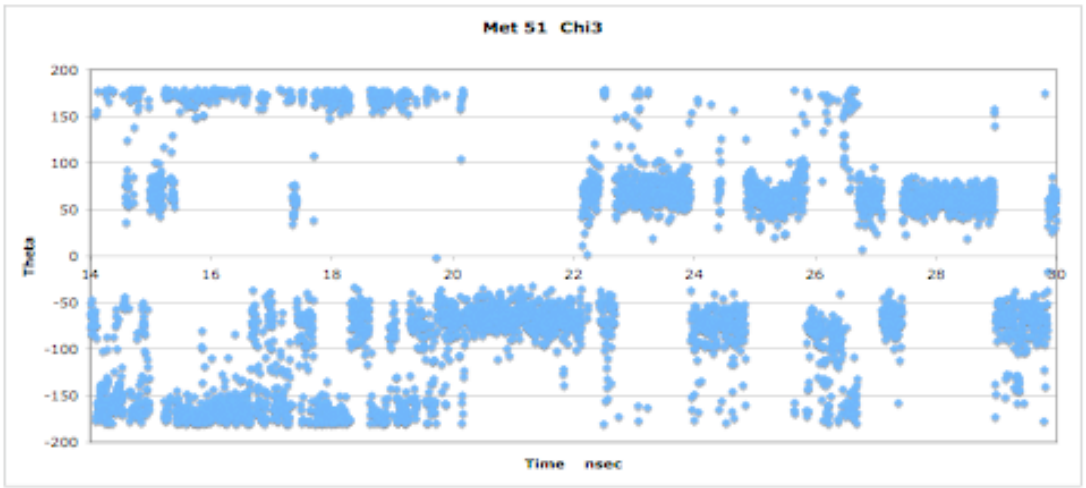
Met 51 Chi3
Theta
Time nsec

M71

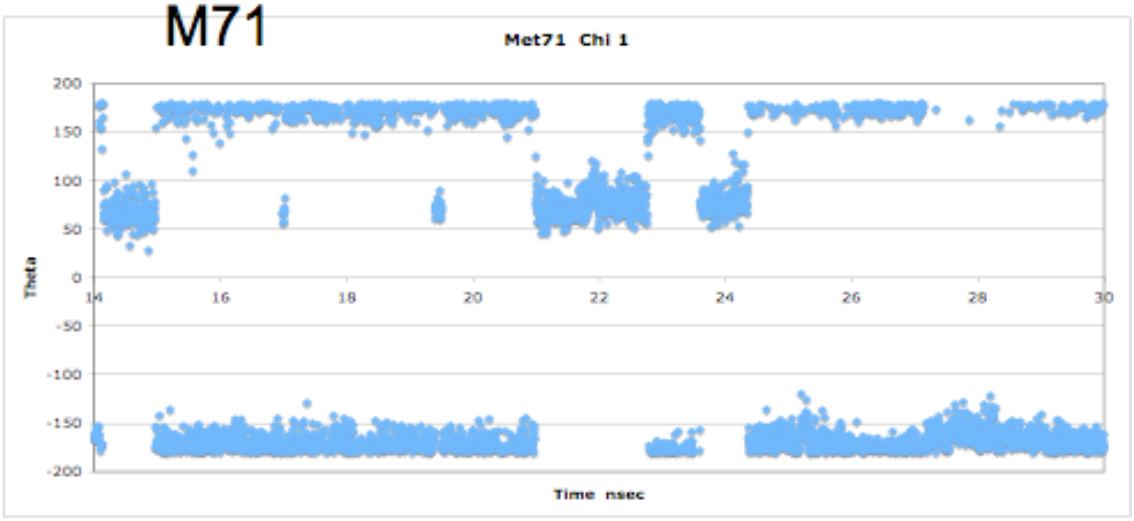
Met71 Chi 1
Theta
Time nsec

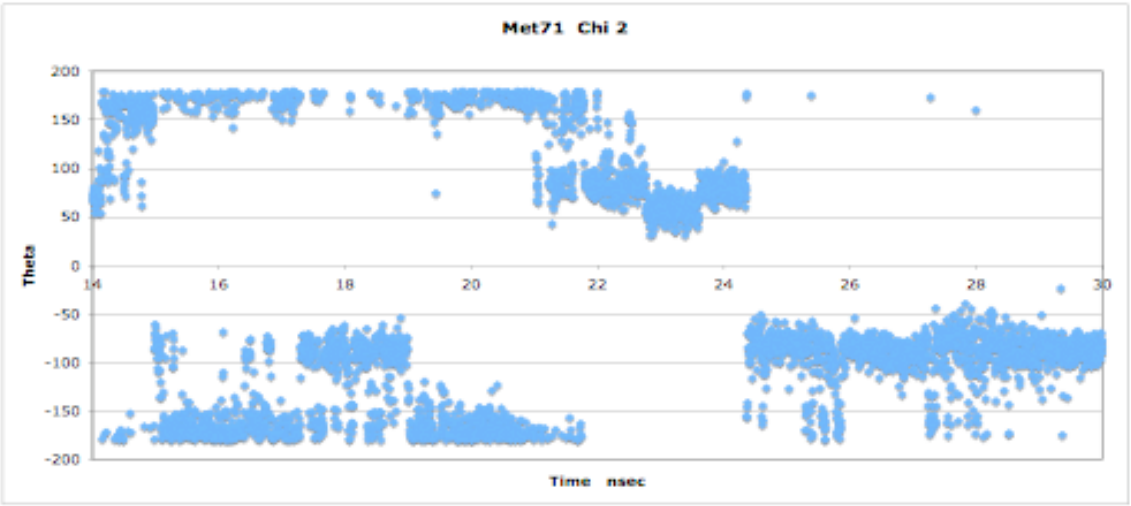
Met71 Chi 2
Theta
Time nsec

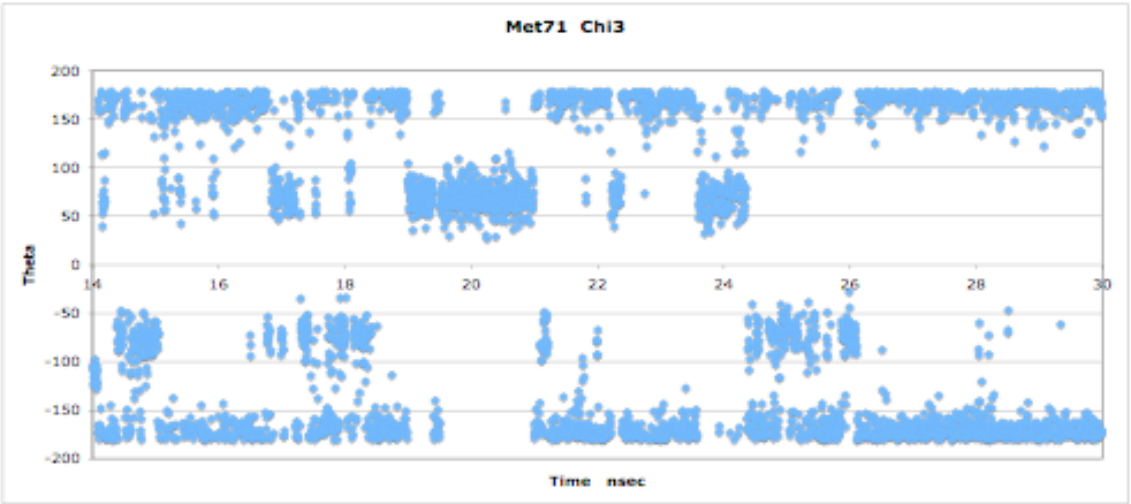
Met71 Chi3
Theta
Time nsec

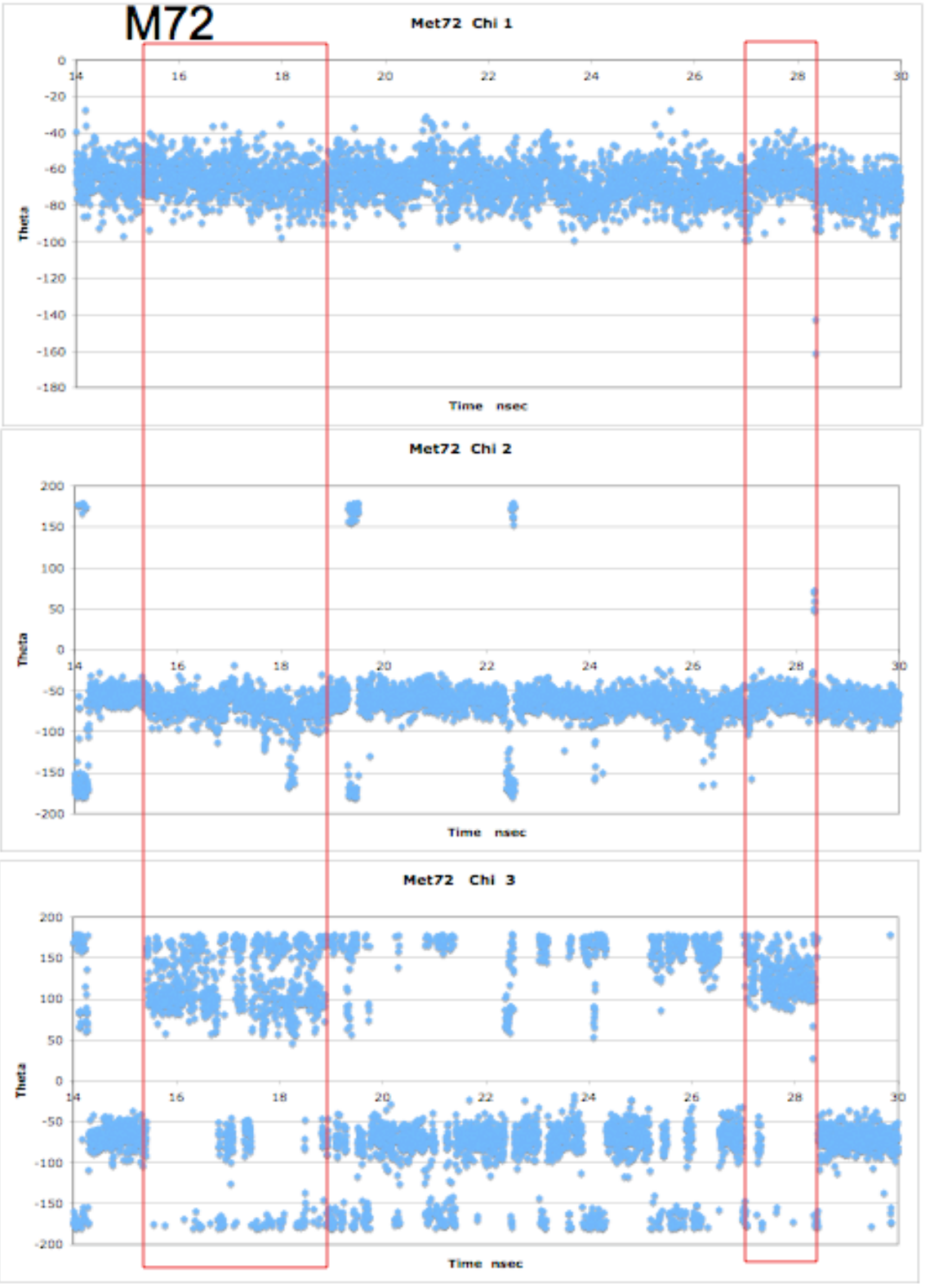
M72
Met72 Chi 1
Theta
Time nsec
Met72 Chi 2
Theta
Time nsec
Met72 Chi 3
Theta
Time nsec

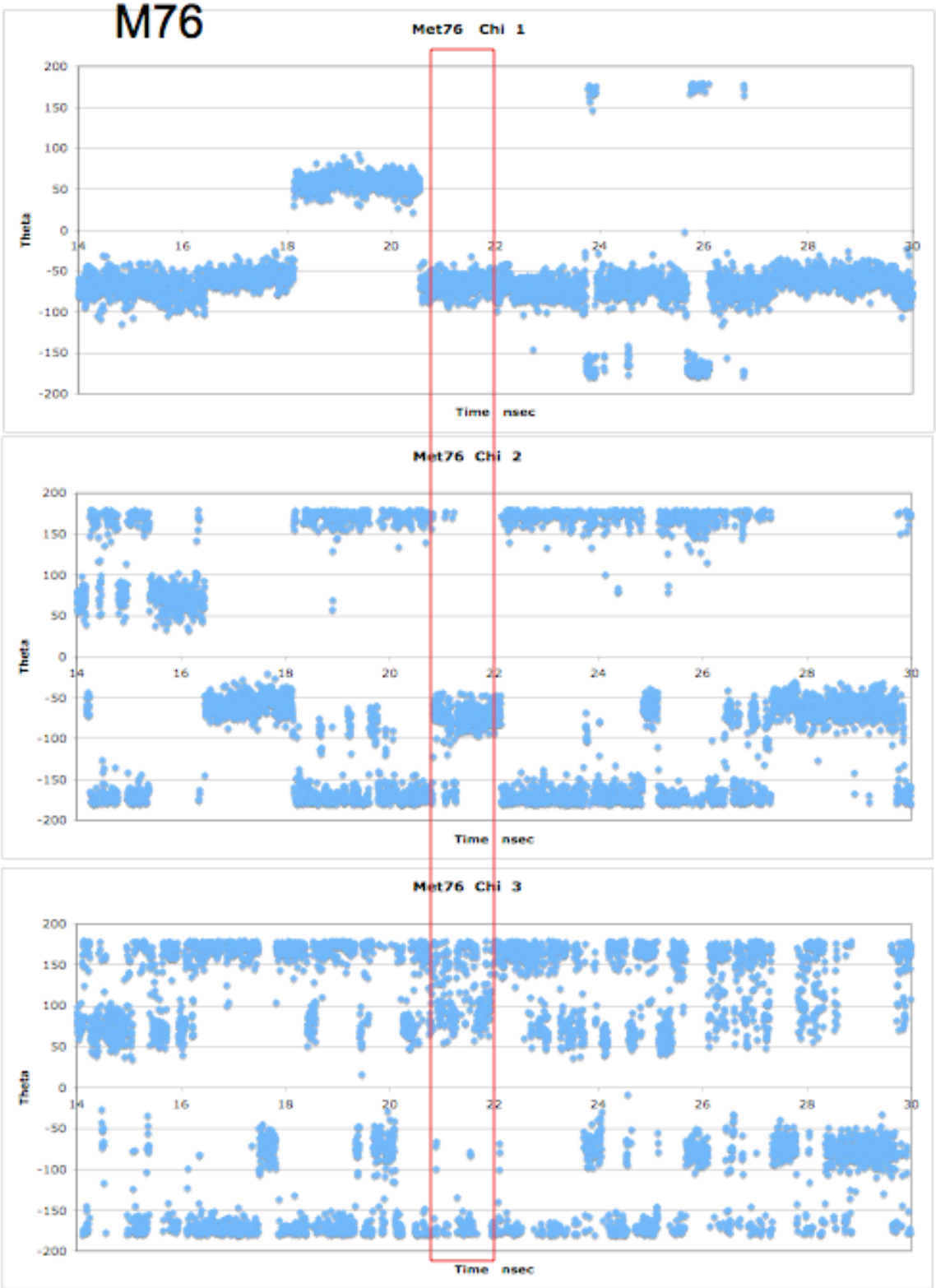
M76
Met76 Chi 1
Theta
Time nsec
Met76 Chi 2
Theta
Time nsec
Met76 Chi 3
Theta
Time nsec

M109

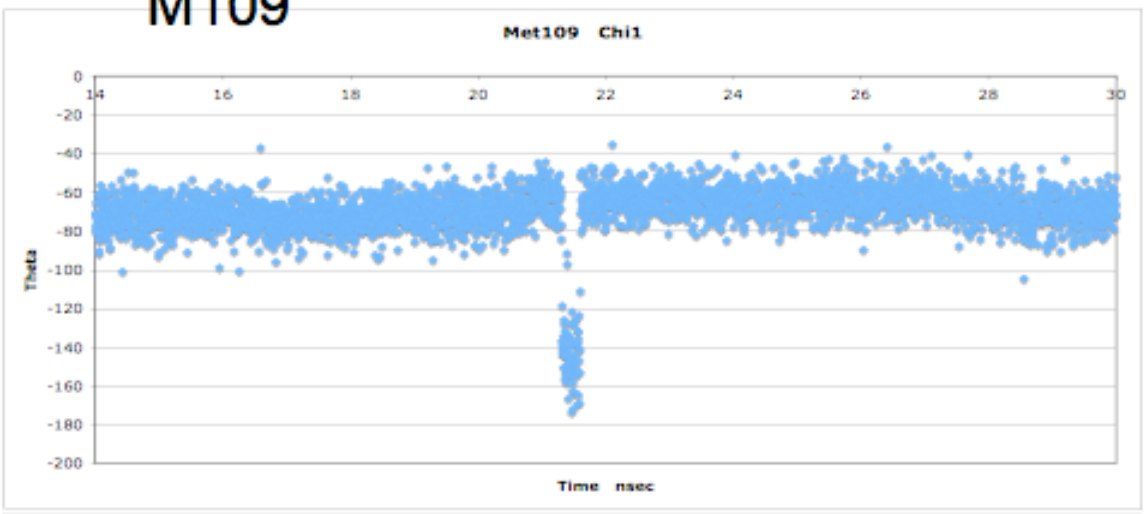
Met109 Chi1
Theta
Time nsec

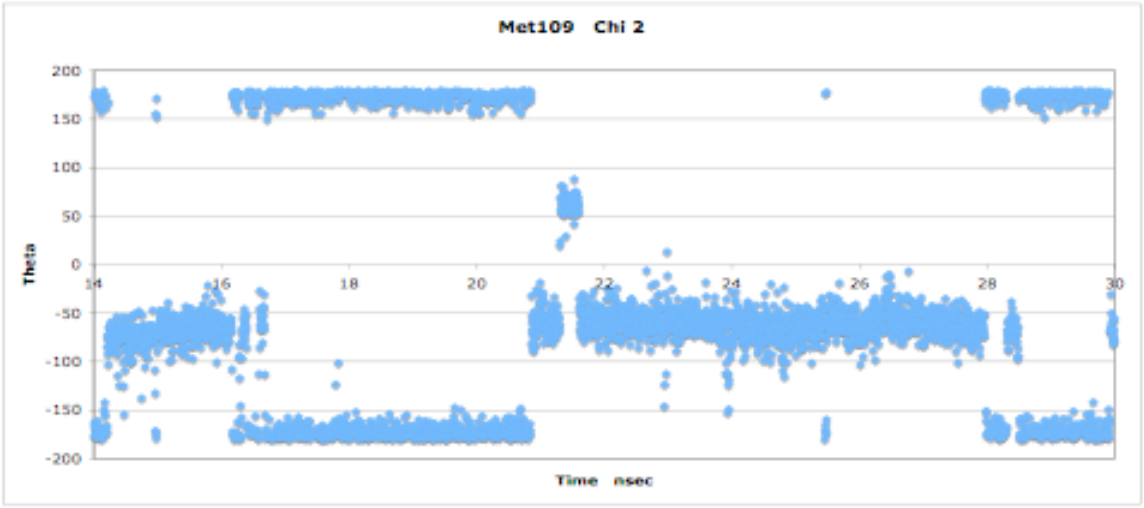
Met109 Chi 2
Theta
Time nsec

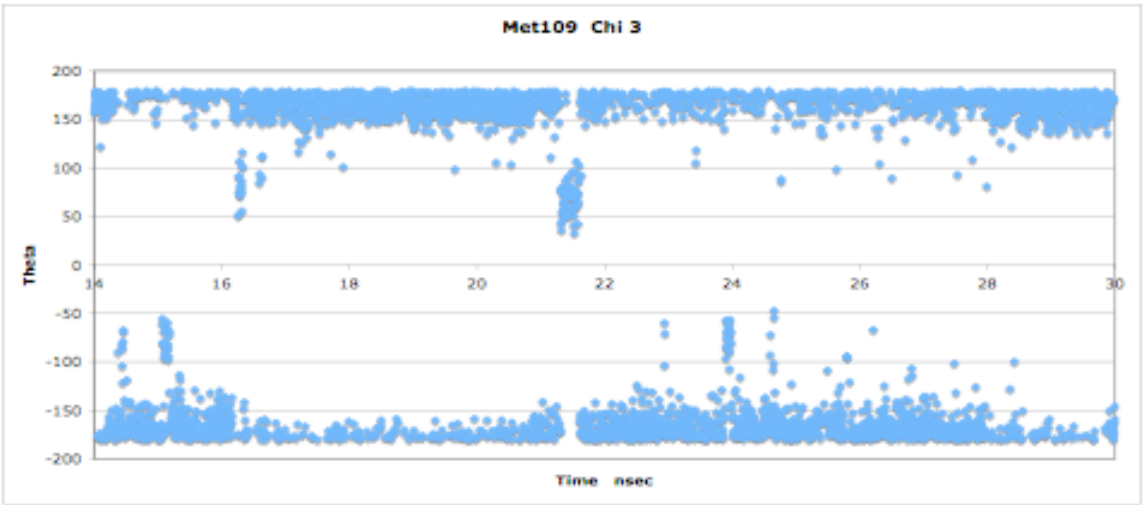
Met109 Chi 3
Theta
Time nsec

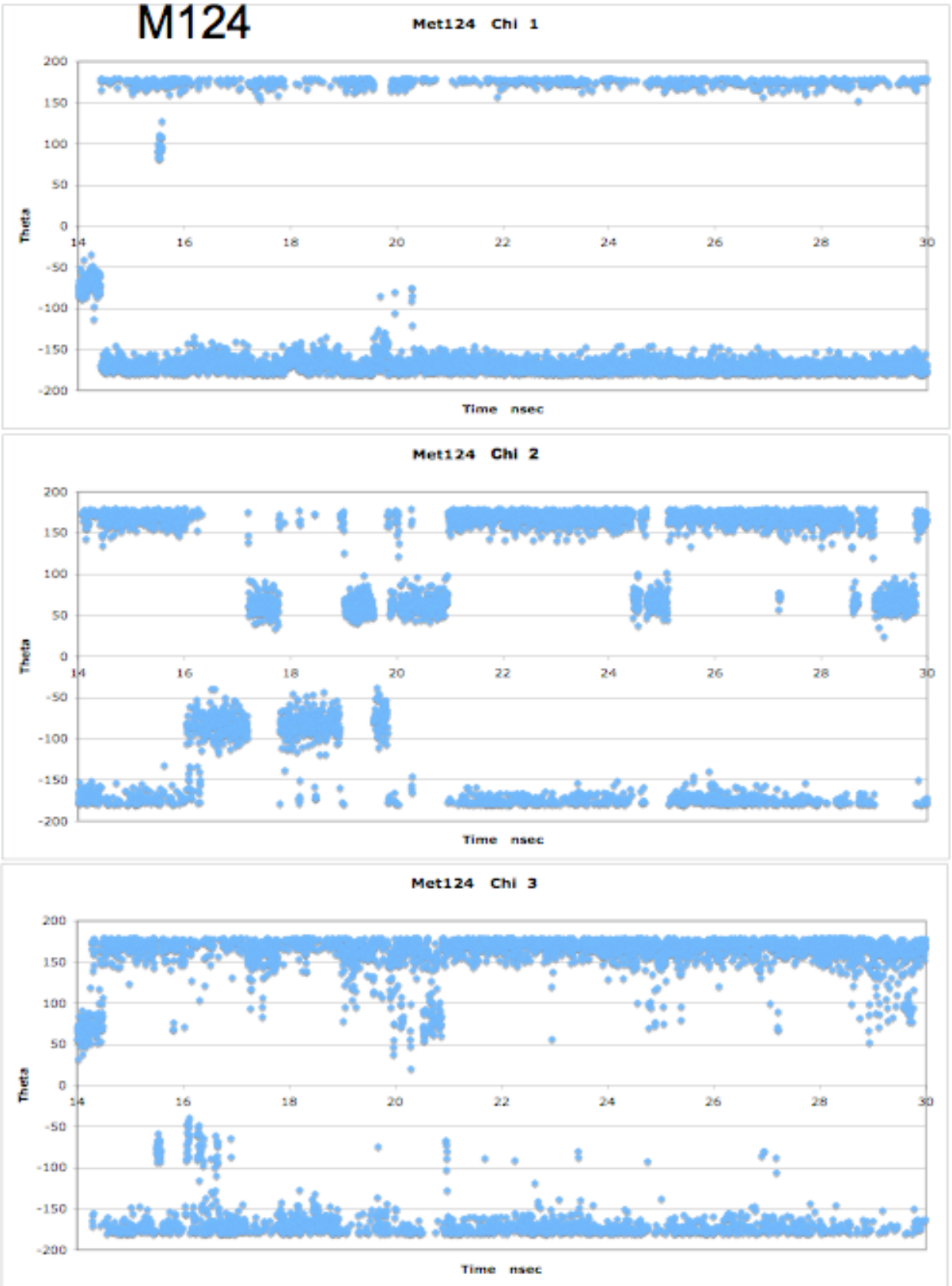
M124
Met124 Chi 1
Theta
Time nsec
Met124 Chi 2
Theta
Time nsec
Met124 Chi 3
Theta
Time nsec

M144

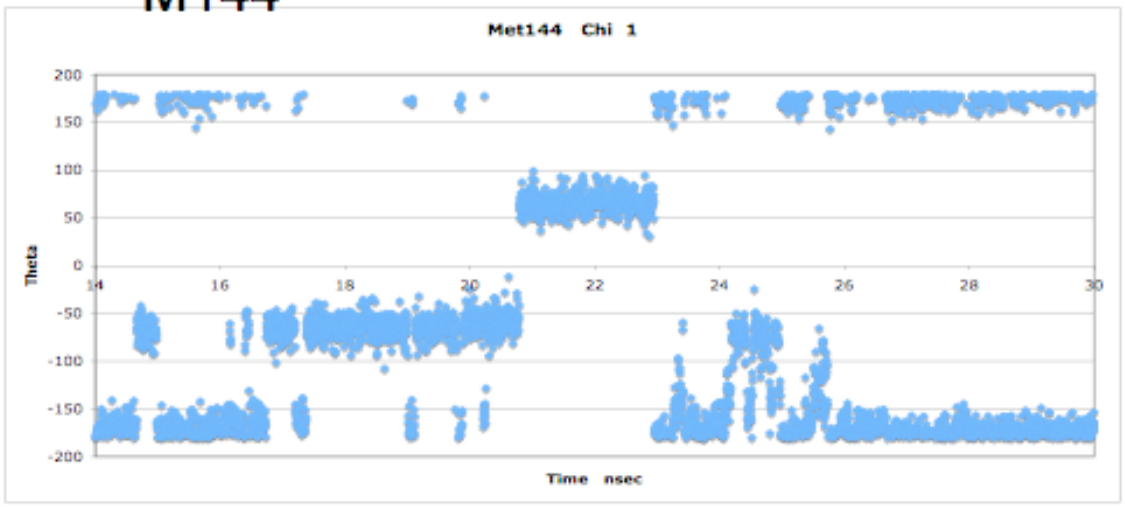
Met144 Chi 1
Theta
Time nsec

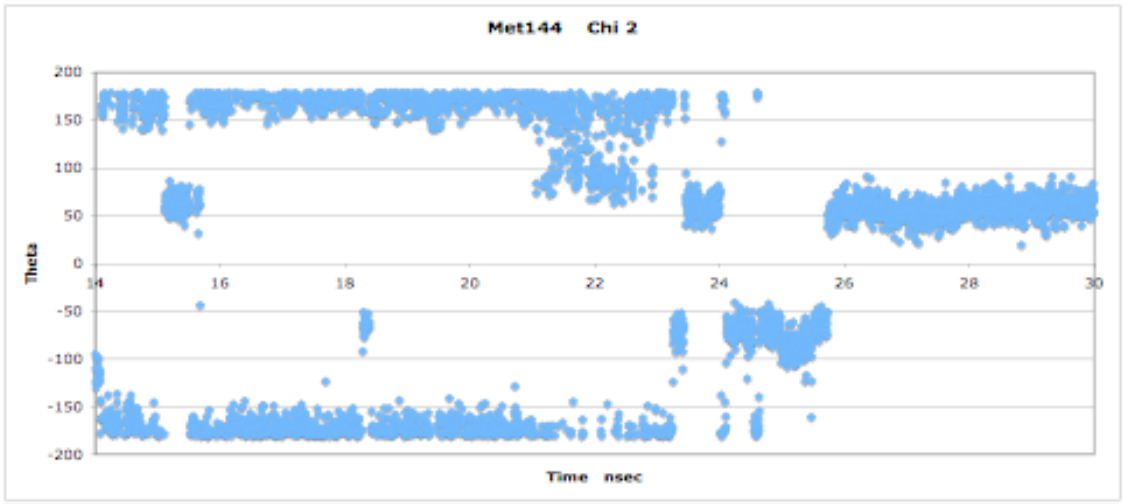
Met144 Chi 2
Theta
Time nsec

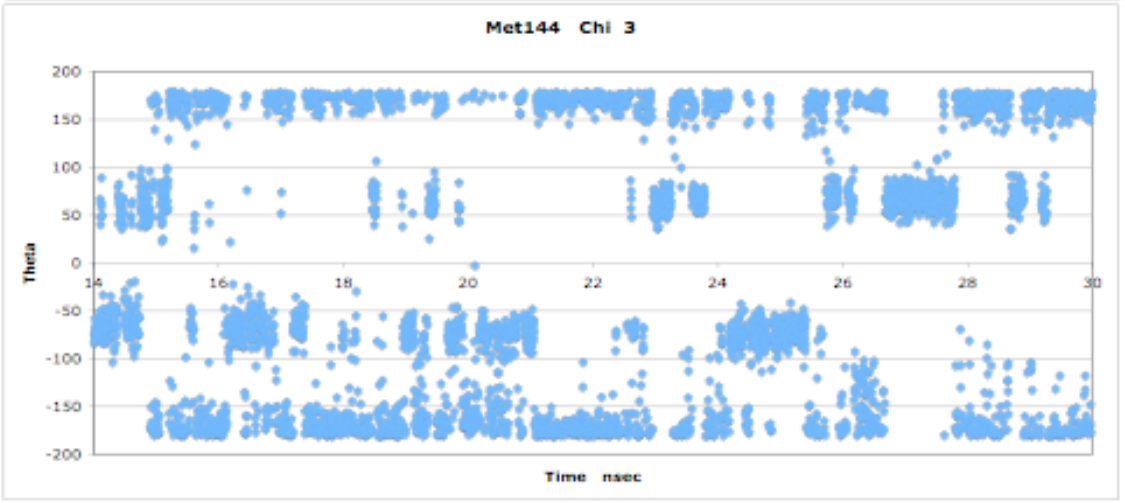
Met144 Chi 3
Theta
Time nsec

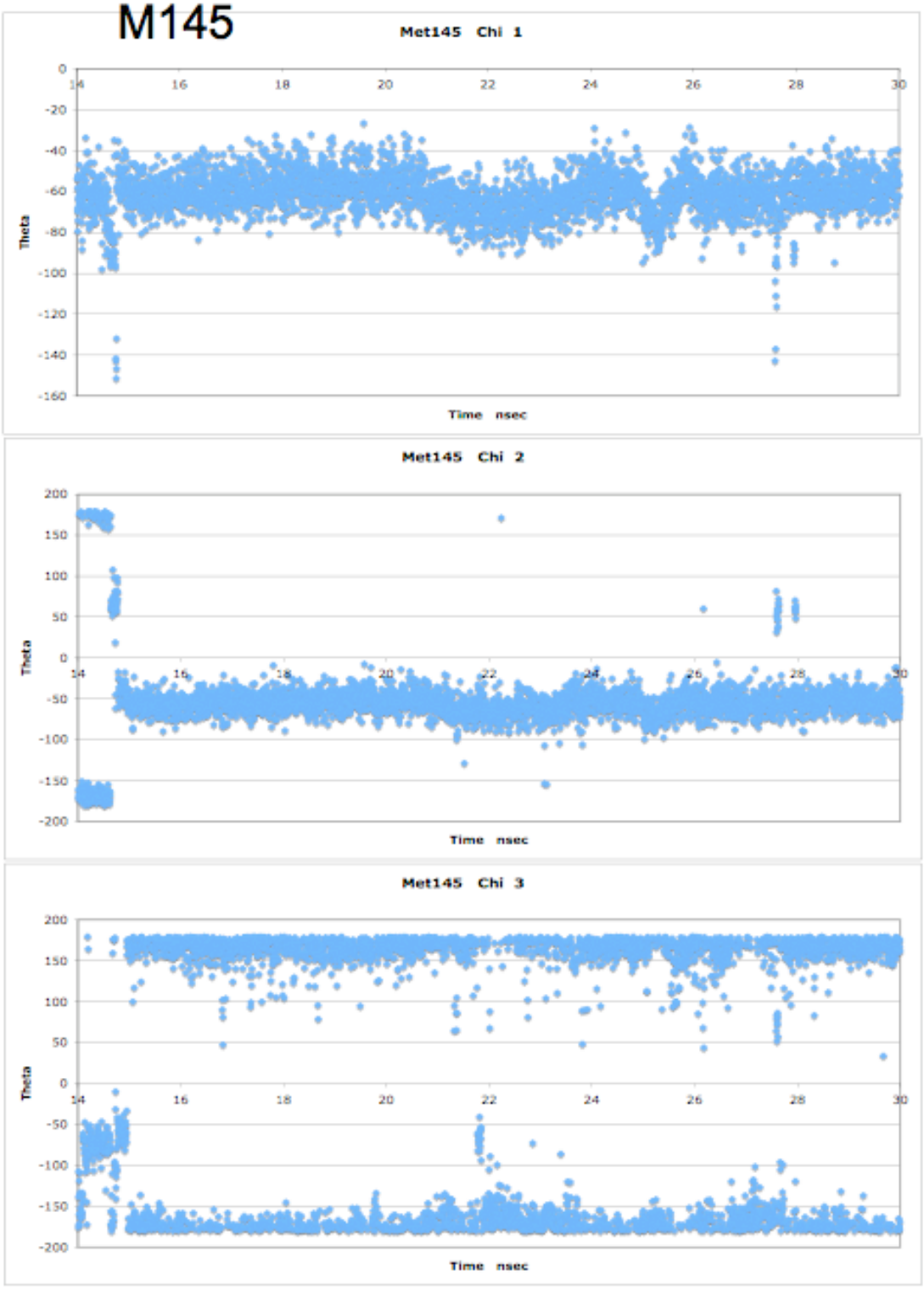
M145
Met145 Chi 1
Theta
Time nsec
Met145 Chi 2
Theta
Time nsec
Met145 Chi 3
Theta
Time nsec

VII: Electric field effecs on S-$^{13}CH_3$ shifts

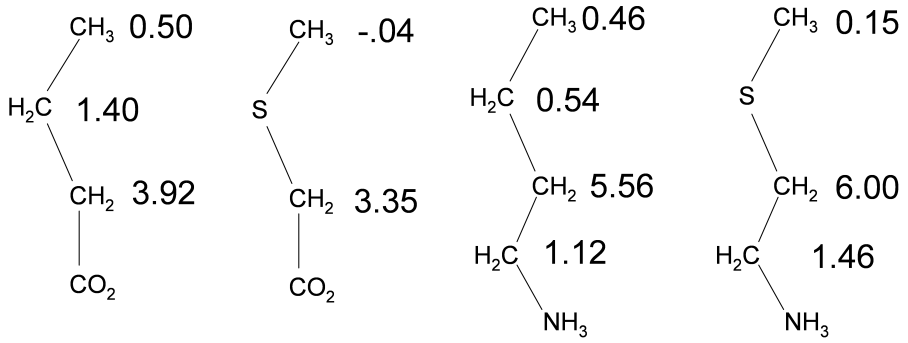

The numbers in the above figure are the $\Delta^{13}C = \delta^{13}C$(deprotonated state) – $\delta^{13}C$ (protonated state). As is apparent from these results, the $\Delta^{13}C$ values for the S-CH_3 containing molecules (methylthio)acetate and 2-(methylthio)ethylamine), are substantially lower than observed for the aliphatic analogs. This behavior probably results primarily from the greater conformational heterogeneity of the sulfur-containing analogs, which will tend to average the electric field polarizations over a wider distribution of orientations. Titration data for the methyl group of 2-(methylthio) ethylamine is shown below:

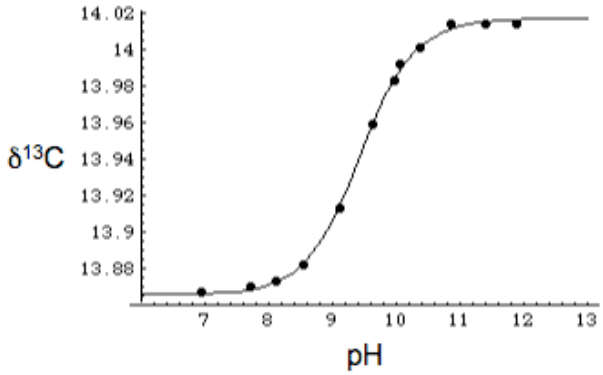

Figure S5. Titration ^{13}C shift of the methyl resonance of 2-(methylthio)ethylamine (the fourth molecule pictured above) as a function of pH.

VIII: Solvent effect on the shift of the methyl resonance of methylthiopropanol

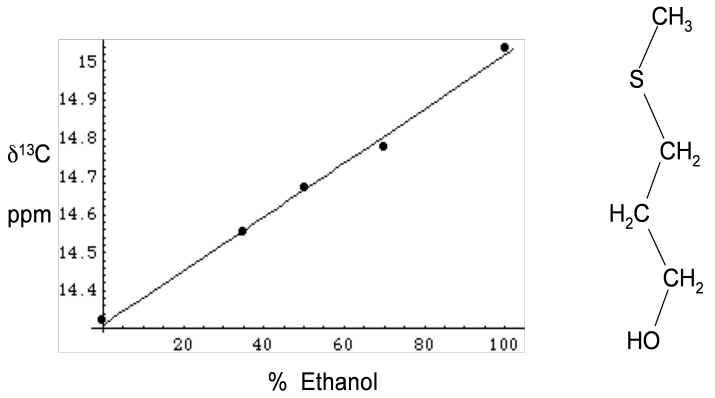

Figure S6. ^{13}C shift of the methyl resonance of 3-(methylthio)-1-propanol as a function of solvent composition. The % ethanol-d6 (v/v) was varied as indicated. Methylthiopropanol was selected for this study due to its solubility in both water and organic solvents. The spectrometer was locked on external D_2O, present in an outer capillary. The observed solvent dependence is small compared with the conformationally-dependent shift derived from the DFT calculations.

IX: Effect of lattice contacts on a buried methionine residue – transferrin residue M109

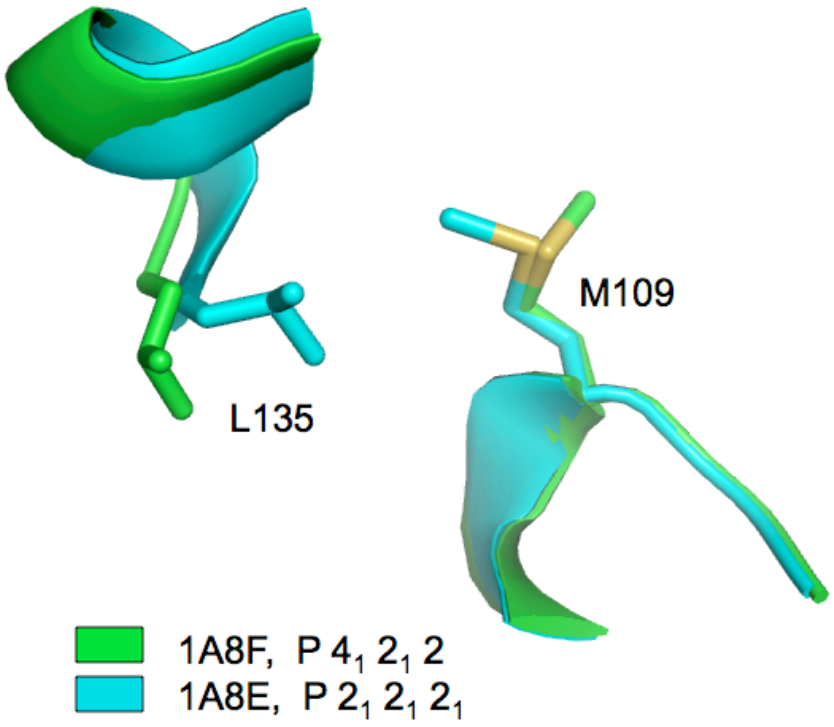

Figure S6. The figure shown above illustrates how crystal packing can influence even the conformation of a buried methionine residue. Structure 1A8E crystallized in the P 2_1 2_1 2_1 space group (cyan), while structure 1A8F crystallized in the P 4_1 2_1 2 space group (green). The two structures shown correspond to the N-lobe of human transferrin (MacGillivray et al. Biochemistry 37, 7919-7928; 1998). Different lattice interactions in the two different space groups alter the position of a loop containing residue L135, and this in turn alters the conformation of buried methionine residue M109.